Supporting Information for

Human Friendly Semitransparent Organic Solar Cells Achieving High Performance

Zonghao Wu[1,3,‡], Beibei Shi[1,3,‡], Jiangsheng Yu[2,4], Mengzhen Sha[1], Jiangkai Sun[1], Dongcheng Jiang[1], Xin Liu[4], Wenxiao Wu[10], Yang Tan[1], Huiyuan Li[11], Shufen Huang[1], Jingjing Wang[5], Junwei Liu[5], Chao Zhang[9], Xiaoling Ma[6], Liyong Cui[7], Long Ye[5], Fujun Zhang[6], Bingqiang Cao[8], Yuguo Chen[10], Ziwu Ji[3,*], Feng Chen[1], Xiaotao Hao[1,*], Gang Li[2,*], Hang Yin[1,*]

[1] School of Physics, State Key Laboratory of Crystal Materials, Shandong University, Jinan, Shandong 250100, China
[2] Department of Electric and Electronic Engineering, Research Institute for Smart Energy (RISE), Photonic Research Institute (PRI), The Hong Kong Polytechnic University, Kowloon, Hong Kong 999077, China
[3] School of Integrated Circuits, Shandong University, Jinan, Shandong 250100, China
[4] School of Electronic and Optical Engineering, Nanjing University of Science and Technology, Nanjing, Jiangsu 210094, China
[5] School of Materials Science & Engineering, Tianjin Key Laboratory of Molecular Optoelectronic Sciences, Tianjin University, Tianjin 300350, China
[6] Key Laboratory of Luminescence and Optical Information, Ministry of Education, Beijing Jiaotong University, Beijing 100044, China
[7] Hunan Provincial Laboratory of Flexible Electronic Materials Genome Engineering, Changsha University of Science and Technology, Changsha 410014, China
[8] School of Material Science and Engineering, University of Jinan, Shandong 250022, China
[9] School of Physics and Electronics, Shandong Normal University, Jinan 250014, China
[10] Department of Emergency Medicine, Qilu Hospital of Shandong University, Jinan, Shandong 250012, China
[11] Department of Ophthalmology, Shandong Provincial Hospital Affiliated to Shandong First Medical University, Jinan, Shandong 250021, China

‡ These authors contributed equally to this work and should be considered co-first authors.

Authors to whom correspondence should be addressed: [Ziwu Ji, jiziwu@sdu.edu.cn; Xiaotao Hao, haoxt@sdu.edu.cn; Gang Li, gang.w.li@polyu.edu.hk and Hang Yin, hyin@sdu.edu.cn]

Supplemental Experimental Procedures

1. Device Fabrication

ITO-coated glass substrates (15 Ω sq^{-1}) were cleaned via sequential ionization in detergent, deionized water, acetone, and isopropanol. All pre-cleaned ITO substrates were treated by oxygen plasma for 180 seconds to increase work function and clearance. PEDOT: PSS layer (30 nm) was spin-coated at a speed of 3500 rpm onto the ITO glass, and annealed at 150 for 15 min. For the binary system, PM6: BTP-eC9 was dissolved in chlorobenzene with a total concentration of 22 mg ml^{-1} (D: A =1:1.2), 20 mg ml^{-1} (D: A = 0.8: 1.2). For the ternary system, PM6: BTP-eC9: L8-BO were dissolved in chlorobenzene with a total concentration of 20 $mgml^{-1}$ (D: A: A= 0.8: 1: 0.2). The solutions were stirred at room temperature. Before spin-coating the active layer, 1,8-diiodooctane (DIO, 0.5% v/ v) was added. The active layer film was spin-coated on the PEDOT: PSS layer in a nitrogen-filled glove box and thermal annealing treatment at 100 °C for 10 min. Then methanol solution of PDINN at a concentration of 1.0 mg ml^{-1} was deposited on the active layer at 3000 rpm for 30 s to afford a cathode buffer layer.

The ultrathin Ag rear electrode is evaporated via a thermal evaporator through a shadow mask with a rate of 3.0 Å s^{-1} under 2.0×10^{-4} Torr, which defines the active cell area of 0.04 cm^2 through an optical microscope. ARC, ABPF and bule light filter were formed by alternate deposition of LiF and TeO_2, and were grown by vacuum thermal evaporation in a chamber with a base pressure of 2.0×10^{-6} Torr at 2.0 Å s^{-1} for LiF and 1.0 Å s^{-1} for TeO_2.

2. Film Fabrication

Organic photovoltaic film: The polymer donors and non-fullerene acceptors were purchased from Solarmer, Inc. without further purification. For BHJ films fabrication, the donor and acceptor were dissolved in chlorobenzene with weight ratio of 1:1 or 1:1.2 at a polymer concentration of 20 or 22 mg/mL. The solution was stirred at room temperature overnight and was spin coated on 1 nm thick quartz substrates with

different speeds to form BHJ films with thickness about 100–200 nm.

Perovskite photovoltaic film: For deposition of $MAPb(I_{1-x}Br_x)_3$ perovskite thin films on 1 nm thick quartz substrates, $MAPb(I_{1-x}Br_x)_3$ precursor solutions ($MAPb(I_{1-x}Br_x)_3$, X = 0, 0.2, 0.4, 0.6, 0.8 and 1) were prepared by the stoichiometric mixing of the bromide and iodide stock solutions (1M of $MAPbBr_3$ and 1M of $MAPbI_3$ in DMF/DMSO (8:2 v/v)). The resulting solution was at room temperature for 2 h with vigorous stirring. The resulting solution was then deposited onto the substrate by a single-step spin-coating process at 3,000 rpm for 30 s. The resulting films were annealed at 100 ℃ for 10 min for better crystallization.

For deposition of $FAPb(I_{1-x}Br_x)_3$ perovskite thin films on 1 nm thick quartz substrates, $FAPb(I_{1-x}Br_x)_3$ precursor solutions ($FAPb(I_{1-x}Br_x)_3$, X = 0, 0.2, 0.4, 0.6, 0.8 and 1) were prepared by the stoichiometric mixing of the bromide and iodide stock solutions (1M of $FAPbBr_3$ and M of $FAPbI_3$ in DMF/DMSO (8:2 v/v)). The resulting solution was at room temperature for 2 h with vigorous stirring. The resulting solution was then deposited onto the substrate by a single-step spin-coating process at 3,000 rpm for 30 s. The resulting films were annealed at 100 ℃ for 10 min for better crystallization.

For control of perovskite film thickness, the concentration of the perovskite precursor solution (1.0 M, 0.7 M, 0.5M, 0.3 M) was adjusted by appropriate dilution with the DMF/DMSO (8:2 v/v) co-solvent blend.

Quantum dot photovoltaic film: 6 mmol PbI_2 and 1 mmol diphenyl thiourea (DPhTA) were dissolved in 9 mL dimethylformamide (DMF) with stirring under argon at a control temperature of ≈ 20 °C. After all solid reagents were dissolved within ≈ 20 min, 1 mL butylamine (BA) was quickly injected to trigger the PbS colloidal quantum dot (CQD) synthesis reaction. After reacting≈9 min, 0.7 mmol tetrabutylammonium iodide (TBAI) in 1 mL DMF was injected into the reaction system and subsequently, the solution was centrifuged for 5 min at 12 000 rpm with the addition of 25 mL toluene. Subsequently, the prepared PbS CQDs in DMF (700 mg/mL) was spincoated with different speeds to form 180-200 nm CQD films in glove box, followed by 75 °C annealing for 15 min.

For other quantum dot photovoltaic films, we cited the data provided in the literature.[1]

Dye-sensitized photovoltaic film: We cited the data provided in the literature.[2-3]

3. Device Characterizations

Device performance was measured in a glove box. To improve the accuracy of measurement, the J-V curves of all devices were measured by masking the active area with a metal mask of 0.0324 cm^2, which defines the illumination area to be 0.0324 cm^2. The J–V curves of devices were determined under AM 1.5G illumination (100 mW cm^{-2}) using a computer-controlled Keithley 2400 source measurement unit and a calibrated solar simulator (Enli Technology Co. Ltd), and no applied bias or light soaking process was applied before J-V measurement. A standard Si secondary reference cell cover with a KG-5 filter was utilized to calibrate the illumination intensity, giving a value of 100 mW cm^{-2} in the test. The J-V curves reported in this manuscript were tested by sweeping the J-V measurement from the forward direction (from short-circuit to open-circuit) with a step of 0.02 V. The delay time is set to zero. EQE were measured by Solar Cell Spectral Response Measurement System QER3011 (Enlitech). The thickness was measured from a Bruker DektakXT Surface Profiler. The absorption spectra and transmittance spectra were measured by the Agilent Cary 5000 spectrophotometer.

4. Optical Simulation

Optical modeling with the transfer matrix method was employed to calculate the transmittance, optical electric field intensity, and exciton generation rate distribution in devices.[4] All the simulations of optical properties and exciton generation are based on the assumptions of planar interfaces and isotropy for the layers within the devices.[5] The optical properties of each layer are represented by the indexes of refraction ($\eta + i\kappa$), measured using a variable angle spectroscopic ellipsometer (WVASE32, J. A. Woollam, VB400). To calculate the exciton generation rate, theoretical maximum photocurrent density and loss portion in the simulated J_{SC}, 100% IQE, and the AM1.5 intensity spectrum (ASTM G173–03) are assumed. The generation of excitons in the active layer is described by considering the following parameters: the modulus squared

of the electric field obtained from TMM, the AM1.5G spectrum, the real part of the refractive index (η), and the absorption coefficient (α), which is associated to the imaginary part (κ) of the refractive index by $\alpha = 4\pi\kappa/\lambda$ and the factor $c\varepsilon_0/2$, where c is the speed of light in vacuum and ε_0 the permittivity of free space.

5. Light Hazard (based on standard IEC 62471:2006/ CIE S 009:2002)

Actinic UV hazard. Prolonged exposure to radiation between 200-400nm wavelengths range can cause skin aging, erythema, and even skin cancer. Therefore, the exposure time to light of this wavelength should be less than t_s, which can be expressed as

$$t_s = \frac{30}{\sum_{200}^{400} E_\lambda(\lambda) \cdot S_{UV}(\lambda) \cdot \Delta\lambda} \quad (1)$$

where $E_\lambda(\lambda)$ is the spectral irradiance in $W \cdot m^{-2} \cdot nm^{-1}$, $S_{uv}(\lambda)$ is the actinic ultraviolet hazard weighting function (Table S1), Δλ is the bandwidth in nm. The 30 is the actinic UV hazard maximum allowable exposure dose, $\sum_{200}^{400} E_\lambda(\lambda) \cdot S_{UV}(\lambda) \cdot \Delta\lambda$ is the calculation expression for actinic UV hazard dose per unit time.

Near-UV hazard. The accumulation of radiation within the 315-400 nm wavelengths range can lead to cataract, with a specified exposure time t_{UVA}, which can be expressed as

$$t_{UVA} = \frac{10000}{\sum_{315}^{400} E_\lambda(\lambda) \cdot \Delta\lambda} \quad (2)$$

where $E_\lambda(\lambda)$ is the spectral irradiance in $W \cdot m^{-2} \cdot nm^{-1}$ and Δλ is the bandwidth in nm. The 10000 is the near-UV hazard maximum allowable exposure dose, $\sum_{315}^{400} E_\lambda(\lambda) \cdot \Delta\lambda$ is the calculation expression for near-UV hazard dose per unit time.

Blue light hazard. Light within the 400-700 nm wavelengths range can cause blue light hazard in humans, resulting in visual fatigue, disrupted circadian rhythms, and even blindness. The corresponding exposure time t_B can be expressed as

$$t_B = \frac{100}{\sum_{300}^{700} E_\lambda(\lambda) \cdot B(\lambda) \cdot \Delta\lambda} \tag{3}$$

where $E_\lambda(\lambda)$ is the spectral irradiance in $W \cdot m^{-2} \cdot nm^{-1}$, $B(\lambda)$ is the blue light hazard weighting function (Table S2), $\Delta\lambda$ is the bandwidth in nm. The 100 is the blue light hazard maximum allowable exposure dose, $\sum_{300}^{700} E_\lambda(\lambda) \cdot B(\lambda) \cdot \Delta\lambda$ is the calculation expression for blue light hazard dose per unit time.

Retinal thermal hazard. To protect against retinal thermal injury, the duration of human eye exposure to light with wavelengths between 380-1400 nm should not exceed the exposure time t_R, which can be expressed as

$$t_R^{0.25} = \frac{50000}{\alpha \cdot \sum_{380}^{1400} L_\lambda(\lambda) \cdot R(\lambda) \cdot \Delta\lambda} \tag{4}$$

where $L_\lambda(\lambda)$ is the spectral radiance in $W \cdot m^{-2} \cdot sr^{-1} \cdot nm^{-1}$, $R(\lambda)$ is the burn hazard weighting function (Table S3), $\Delta\lambda$ is the bandwidth in nm and α is the angular subtense of the source in radians. $\sum_{380}^{1400} L_\lambda(\lambda) \cdot R(\lambda) \cdot \Delta\lambda$ is the calculation expression for retinal thermal hazard dose per unit time. Based on the IEC 62471:2006/CIE S 009:2002 document, $L_\lambda(\lambda)$ can be computationally substituted by $E(\lambda)$ multiplied by a factor of 10,000. Therefore, we use the AM 1.5G solar spectrum multiplied by 10000 in place of $L_\lambda(\lambda)$ for the blue light hazard analysis.

Infrared radiation hazard. Exceeding the exposure time t_{IR} for exposure of human

eyes to light within the 780-3000 nm range can lead to corneal burn and cataract. The corresponding exposure time t_{IR} can be expressed as

$$t_{IR}^{0.75} = \frac{18000}{\sum_{780}^{3000} E_{\lambda}(\lambda) \cdot \Delta\lambda} \tag{5}$$

where $E_{\lambda}(\lambda)$ is the spectral irradiance in $W \cdot m^{-2} \cdot nm^{-1}$ and $\Delta\lambda$ is the bandwidth in nm. $\sum_{780}^{3000} E_{\lambda}(\lambda) \cdot \Delta\lambda$ is the calculation expression for infrared radiation hazard dose per unit time.

Thermal hazard. To protect against skin burns, the duration of human skin exposure to light with wavelengths between 380-3000nm should not exceed the exposure time t_H, which can be expressed as

$$t_{H}^{0.75} = \frac{20000}{\sum_{380}^{3000} E_{\lambda}(\lambda) \cdot \Delta\lambda} \tag{6}$$

where $E_{\lambda}(\lambda)$ is the spectral irradiance in $W \cdot m^{-2} \cdot nm^{-1}$ and $\Delta\lambda$ is the bandwidth in nm. $\sum_{380}^{3000} E_{\lambda}(\lambda) \cdot \Delta\lambda$ is the calculation expression for thermal hazard dose per unit time. It is important to note that t_H applies only to small area irradiation. T_H is not applicable for large area irradiation, as it involves heat exchange between the individual and the environment, physical activity, and various other factors. Therefore, this work only analyzes the hazard level of thermal radiation, rather than the exposure time.

6. Optical Properties

AVT. The average visible light transmittance (AVT) are calculated according to the equation:

$$AVT = \frac{\int T(\lambda) \cdot V(\lambda) \cdot AM1.5G(\lambda)\, d(\lambda)}{\int V(\lambda) \cdot AM1.5G(\lambda)\, d(\lambda)} \quad (7)$$

Where $T(\lambda)$ is the transmission spectrum, $V(\lambda)$ is the photopic response of human eye, $AM1.5G(\lambda)$ is photon flux.

CRI. The CRI value is defined as the value from 0 to 100, a higher CRI represents better color rendering ability and higher neutral color degree. The CRI can be evaluated according to the matching degree between the transmitted light from the devices and the illumination light.

Table S1. Light hazard with different wavelengths.

Light hazard	Wavelength (nm)	Hazardous effect	
		Eyes	Skin
Actinic UV hazard	200-400	Cataracts Keratitis	Photoaging Erythema
Near-UV hazard	315-400	Cataracts	
Blue light hazard	300-700	Circadian rhythm Blindness	
Retinal thermal hazard	780-3000	Cataracts Corneal burn	
Infrared radiation hazard	380-1400	Retinal burn	
Thermal hazard	380-3000		Skin burn

Table S2. Actinic ultraviolet hazard weighting function $S_{uv}(\lambda)$.

Wavelength nm	**UV hazard function Suv(λ)**	**Wavelength nm**	**UV hazard function Suv(λ)**
200	0.030	313	0.006
205	0.051	315	0.003
210	0.075	316	0.024
215	0.095	317	0.0020
220	0.120	318	0.0016

225	0.150	319	0.0012
230	0.190	320	0.0010
235	0.240	322	0.00067
240	0.300	323	0.00054
245	0.360	325	0.00050
250	0.430	328	0.00044
254	0.500	330	0.00041
255	0.520	333	0.00037
260	0.650	335	0.00034
265	0.810	340	0.00028
270	1.000	345	0.00024
275	0.960	350	0.00020
280	0.880	355	0.00016
285	0.770	360	0.00013
290	0.640	365	0.00011
295	0.540	370	0.000093
297	0.460	375	0.000077
300	0.300	380	0.000064
303	0.120	385	0.000053
305	0.060	390	0.000044
308	0.026	395	0.000036
310	0.015	400	0.000030

Table S3. Blue light hazard weighting function B(λ).

Wavelength nm	**Blue light hazard weighting function B(λ)**
300-380	0.01
385	0.013
390	0.025
395	0.05
400	0.10
405	0.20
410	0.40
415	0.80
420	0.90
425	0.95
430	0.98
435	1.00
440	1.00
445	0.97
450	0.94
455	0.90
460	0.80
465	0.70
470	0.62
475	0.55
480	0.45
485	0.40
490	0.22
495	0.16
500-600	$10^{[(450-\lambda)/50]}$
600-700	0.001
>700	0

Table S4. Burn hazard weighting function R(λ).

Wavelength nm	**Burn hazard weighting function R(λ)**
380	0.1
385	0.13
390	0.25
395	0.5
400	1.0
405	2.0
410	4.0
415	8.0
420	9.0
425	9.5
430	9.8
435	10.0
440	10.0
445	9.7
450	9.4
455	9.0
460	8.0
465	7.0
470	6.2
475	5.5
480	4.5
485	4.0
490	2.2
495	1.6
500-700	1.0
700-1050	$10^{[(700-\lambda)/500]}$
1050-1150	0.2
1150-1200	$0.2 \cdot 10^{0.02 \cdot (1150-\lambda)}$
1200-1400	0.02

Table S5. Performance parameters of different films.

Materials	Thickness (nm)	AVT (%) (film)	PCE (%) (gpvdm)	LUE (%) (film)	CRI (film)	Actinic UV hazard ($W \cdot m^{-2}$)	Near-UV hazard ($W \cdot m^{-2}$)	Blue light hazard ($W \cdot m^{-2}$)	Retinal thermal hazard ($W \cdot m^{-2} \cdot sr^{-1}$)	Infrared radiation hazard ($W \cdot m^{-2}$)	Thermal hazard ($W \cdot m^{-2}$)
D18: N3	160	28.77	13.36	3.84	84.1	0.0072	18.74	333.21	45.21	576.48	496.41
	120	38.492	15.32	5.90	88.3	0.0093	23.04	338.87	54.15	697.88	550.42
	100	44.694	15.68	7.01	89.7	0.0107	25.82	342.78	59.41	772.72	586.23
	90	46.861	15.4	7.22	91.0	0.0111	26.59	343.35	60.96	794.39	596.19
PBDB-T: ITIC	150	27.24	8.90	2.42	79.80	0.0095	20.63	409.92	50.89	686.00	603.60
	110	36.66	10.14	3.72	86.73	0.0117	25.23	404.64	59.50	791.84	638.75
	100	42.34	10.81	4.58	88.69	0.0131	27.99	406.23	64.29	854.92	664.98
	90	43.76	10.90	4.77	89.29	0.0135	28.60	406.55	65.20	868.21	671.38
	70	48.88	10.32	5.04	91.02	0.0147	30.61	408.27	68.35	915.23	694.88
PBDB-T: N2200	150	43.31	5.49	2.38	94.70	0.0136	23.76	408.76	60.57	859.82	700.91
	110	50.74	6.34	3.22	96.10	0.0155	27.79	411.81	66.35	936.71	734.66
	100	55.37	6.56	3.63	96.80	0.0165	29.87	414.04	69.17	978.69	756.33
	90	56.18	6.68	3.75	96.90	0.0168	30.40	414.50	69.93	988.68	760.68
	70	59.70	6.42	3.83	97.30	0.0174	31.92	416.44	72.20	1022.99	778.65
PM6: L8-BO	220	12.48	13.80	1.72	87.91	0.0042	10.72	348.89	29.82	389.41	440.87
	160	23.49	14.72	3.46	95.37	0.0071	16.31	360.58	42.15	552.78	512.53
	120	31.68	16.21	5.14	96.32	0.0089	20.13	360.27	50.29	659.53	554.88
	100	37.94	16.67	6.32	96.97	0.0104	23.11	361.47	55.95	735.62	587.31
	90	46.45	13.40	6.22	97.70	0.0126	27.14	365.80	62.84	833.57	633.96
D18:L8-BO	120	27.04	14.50	3.92	60.89	0.0083	18.77	360.12	42.38	581.45	537.40
P3HT: $PC_{71}BM$	110	52.84	3.46	1.83	93.25	0.0103	23.13	413.31	39.24	715.79	737.80
	90	55.75	3.42	1.91	92.61	0.0122	26.55	415.08	45.97	786.92	755.74
	70	59.06	3.22	1.90	92.38	0.0135	28.80	417.09	50.92	845.46	775.63

	60	59.41	2.31	1.37	92.20	0.0137	29.11	417.43	51.51	852.56	778.18
PM6: Y6	220	14.67	11.46	1.68	92.02	0.0045	11.80	335.15	32.07	414.97	441.62
	160	28.74	12.58	3.62	96.49	0.0077	18.53	349.10	47.35	620.39	533.66
	120	33.96	15.00	5.09	96.91	0.0088	20.97	350.98	52.25	686.55	562.21
	100	38.65	15.82	6.11	97.30	0.0099	23.19	353.64	56.56	745.32	588.60
	90	41.66	15.83	6.59	97.65	0.0106	24.66	354.60	58.96	778.38	603.50
	80	44.84	15.41	6.91	97.87	0.0114	26.11	356.90	61.66	816.34	621.56
PBDB-T:BTA3	90	37.51	7.67	2.88	91.36	0.0141	29.31	414.49	62.52	878.85	708.82
PTB7-Th: IEICO-4F	150	36.04	8.44	3.04	72.50	0.0056	17.49	351.15	51.07	632.39	516.17
	110	49.18	10.26	5.05	79.70	0.0082	22.65	361.01	61.18	776.06	586.03
	100	54.97	10.50	5.77	82.70	0.0094	25.08	362.18	65.89	842.04	615.74
	90	55.27	10.43	5.76	82.70	0.0094	25.17	362.35	66.10	844.82	616.93
	80	55.57	10.01	5.56	82.90	0.0095	25.33	361.91	66.34	848.11	618.12
PM6: BTP-eC9	220	12.97	12.34	1.60	90.10	0.0037	9.12	328.16	29.96	387.51	426.12
	160	24.70	15.15	3.74	95.80	0.0063	14.90	340.43	43.31	566.17	505.84
	120	29.38	17.25	5.07	95.80	0.0075	17.14	344.25	48.27	633.62	536.23
	100	30.55	17.46	5.33	96.00	0.0078	17.69	345.02	49.40	648.76	542.80
	90	31.07	17.20	5.34	96.10	0.0078	17.93	344.87	49.84	654.50	545.02
PTB7-Th: $PC_{71}BM$	160	37.64	6.92	2.60	95.88	0.0033	10.69	414.86	31.02	539.38	622.89
	120	49.58	8.08	4.01	96.97	0.0053	15.64	406.88	43.26	687.31	669.41
	100	53.06	8.65	4.59	97.53	0.0063	18.09	406.26	47.76	740.05	685.85
	90	53.73	8.66	4.65	97.63	0.0066	18.59	406.33	48.57	749.88	689.27
	80	54.03	8.37	4.52	97.70	0.0067	18.78	406.40	48.87	753.93	691.02
MG214		15.91	7.01	1.12	31.39	0.0019	2.72	426.53	22.75	467.21	621.12
YKP88		31.75	9.52	3.02	60.34	0.0095	14.83	426.53	41.29	701.69	705.29
YKP137		39.72	9.55	3.79	75.80	0.0029	6.28	426.53	40.06	735.18	741.50
SL9&SL10		14.58	15.20	2.22	35.10	0.0015	3.22	426.53	13.88	397.66	627.93

CdSe580		35.89	10.75	3.86	94.20	0.0014	2.91	395.30	11.81	371.53	606.77
ZClSe		44.05	9.91	4.37	95.10	0.0019	3.95	393.15	19.10	451.72	626.91
PbS		14.65	8.80	1.29	98.90	0.0001	0.23	360.87	2.63	205.74	518.20
PbS colloidal		27.00	5.10	1.38	96.50	0	0.22	363.85	7.23	217.61	517.60
$MAPb(I_{1-x}Br_x)_3$ X=1	120	36.24	9.94	3.60	93.70	0.0014	2.75	424.32	10.86	391.79	645.67
	180	15.80	13.20	2.09	92.70	0.0004	0.62	421.25	2.98	231.59	542.63
	220	14.70	13.43	1.97	88.20	0.0002	0.24	420.53	1.78	213.42	533.38
X=0.8	90	58.94	11.00	6.48	90.70	0.0011	3.07	424.85	19.46	535.10	727.38
	200	16.87	11.89	2.01	90.10	0.0002	0.32	421.26	2.25	234.13	554.29
X=0.6	100	47.39	7.56	3.58	94.10	0.0011	3.31	424.87	16.79	487.33	699.95
	170	24.13	9.26	2.23	90.60	0.0002	0.49	423.05	3.80	294.47	606.35
	240	15.29	12.06	1.84	88.10	0.0001	0.15	420.21	1.31	235.45	563.43
X=0.4	60	69.37	3.83	2.66	97.00	0.0033	10.70	425.99	39.48	769.87	803.52
	100	47.82	5.32	2.54	95.90	0.0011	3.56	423.89	17.91	506.56	710.14
	170	28.37	6.58	1.87	92.70	0.0001	0.54	422.41	5.68	335.66	633.32
X=0.2	80	65.21	2.74	1.79	95.80	0.0011	5.60	424.99	33.14	697.14	778.47
	120	54.94	3.68	2.02	89.30	0.0002	1.41	426.29	17.69	542.74	749.38
X=0	70	68.88	4.33	2.98	92.80	0.0014	6.45	424.71	34.95	718.47	782.72
	90	67.40	4.70	3.17	85.70	0.0008	3.27	424.51	23.92	614.77	768.06
	110	65.88	5.05	3.33	83.40	0.0003	1.82	424.24	19.64	570.36	758.12
$FAPb(I_{1-x}Br_x)_3$ X=1	230	14.53	9.92	1.44	88.60	0.0001	0.21	414.02	1.54	212.20	531.63
	280	12.22	12.11	1.48	88.10	0	0.07	416.56	0.67	210.09	538.14
X=0.8	160	37.87	8.54	3.23	88.70	0.0002	0.69	426.13	5.99	354.52	652.34
	240	27.83	9.67	2.69	84.50	0	0.06	417.87	1.95	279.23	601.42
X=0.6	130	56.68	5.22	2.96	86.30	0.0004	1.40	426.53	10.36	459.29	726.33
	160	55.17	6.96	3.84	76.70	0.0001	0.47	422.91	6.46	397.36	691.65
	190	46.73	6.69	3.13	76.10	0	0.14	422.43	4.10	347.17	657.63

X=0.4	155	42.21	6.63	2.80	92.20	0.0001	0.68	426.53	8.58	421.72	701.75
	215	30.22	7.11	2.15	91.40	0	0.13	421.98	4.12	322.93	633.07
X=0.2	100	57.23	4.85	2.78	90.20	0.0012	3.55	426.53	20.75	578.14	761.40
	170	39.51	6.08	2.40	89.10	0.0002	0.63	424.96	8.90	406.23	681.24
X=0	90	73.32	5.67	4.16	86.40	0.0008	3.39	426.53	26.97	667.42	798.16
	140	58.05	7.44	4.32	79.50	0	0.55	424.38	14.76	494.78	721.06

Table S6. The detailed thicknesses of optical layers for antireflection coating (ARC).

layer	Materials	Thickness (nm)
1	LiF	115.0
2	TeO_2	27.0
3	LiF	22.0
4	TeO_2	134.0
5	LiF	13.0
6	TeO_2	35.0
7	LiF	32.0
8	TeO_2	16.0
9	Glass	-

Table S7. The detailed thicknesses of optical layers for aperiodic band-pass filter (ABPF).

layer	Materials	Thickness (nm)
1	Ag	12.0
2	LiF	145.9
3	TeO_2	89.9
4	LiF	149.2
5	TeO_2	93.7
6	LiF	150.3
7	TeO_2	93.8
8	LiF	150.3
9	TeO_2	93.9
10	LiF	151.2
11	TeO_2	94.7
12	LiF	152.1
13	TeO_2	96.3
14	LiF	154.4
15	TeO_2	99.7
16	LiF	162.8
17	TeO_2	106.5
18	LiF	84.3

Table S8. The detailed thicknesses of optical layers for blue light filter structure.

layer	Materials	Thickness (nm)
1	LiF	135.0
2	TeO_2	190.0
3	LiF	55.0
4	TeO_2	28.0
5	LiF	81.0
6	TeO_2	26.5
7	LiF	51.5
8	TeO_2	40.5
9	LiF	41.5
10	TeO_2	42.5
11	LiF	77.0
12	TeO_2	32.0
13	LiF	95.0
14	TeO_2	48.0
15	LiF	63.0
16	TeO_2	41.0
17	LiF	267.5
18	TeO_2	9.5
19	LiF	25.0
20	TeO_2	172.0
21	LiF	260.0
22	TeO_2	177.5
23	LiF	245.0
24	TeO_2	11.0
25	LiF	27.0
26	TeO_2	184.0

27	LiF	55.0
28	TeO_2	19.0
29	LiF	246.5
30	TeO_2	5.5
31	LiF	66.0
32	TeO_2	17.0
33	LiF	57.0
34	TeO_2	15.5

Table S9. The ST-OPV structure.

layer	Materials	Thickness (nm)
1	ARC	-
2	Glass	-
3	ITO	135.0
4	PEDOT:PSS	30.0
5	Active Layer	75.0
6	PDINN	10.0
7	Ag	12.0
8	ABPF	-
9	UV light filter	-
10	Blue light filter	-

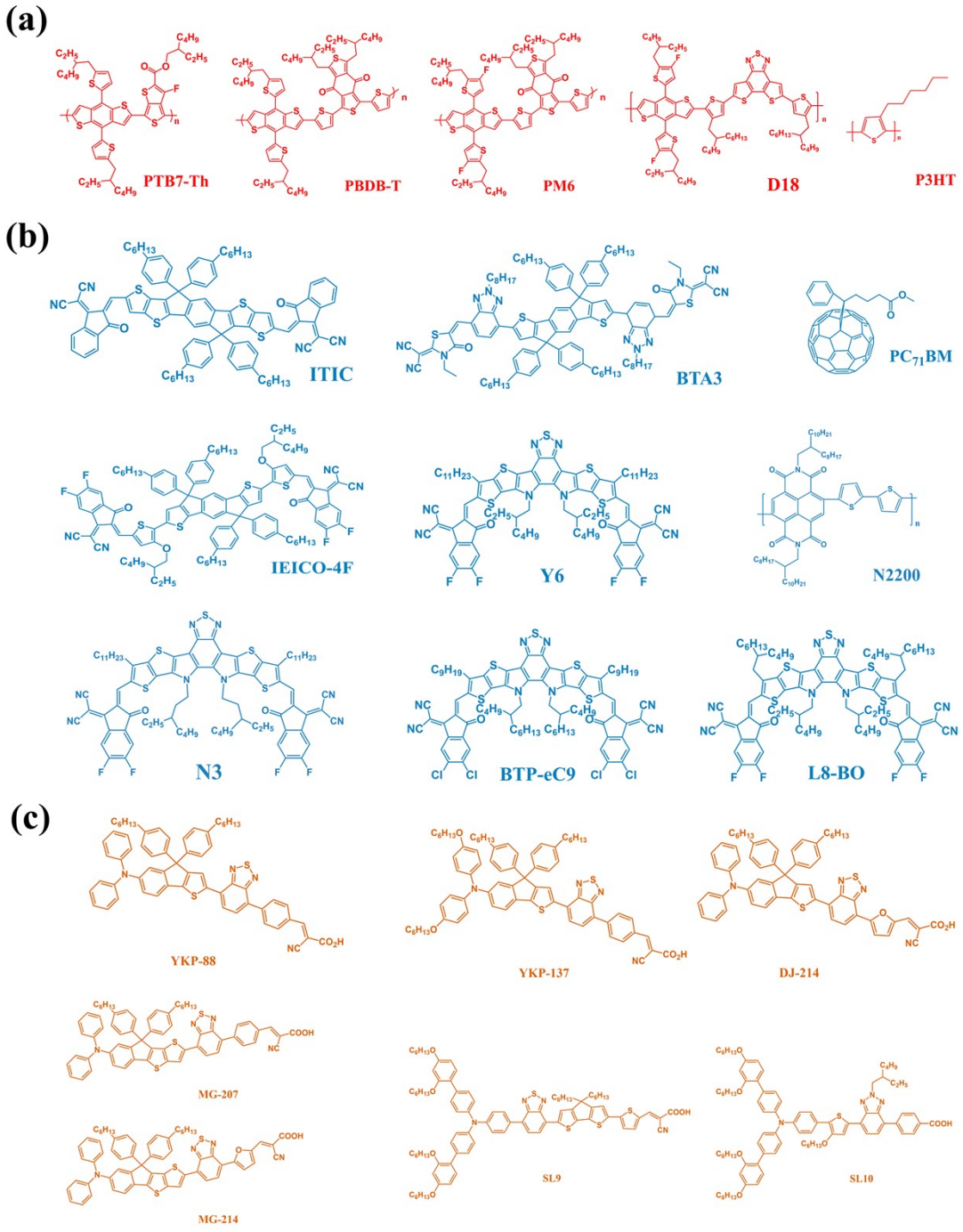

Figure S1. Chemical structures of (a) organic donor materials, (b) organic acceptor materials, and (c) dyes.

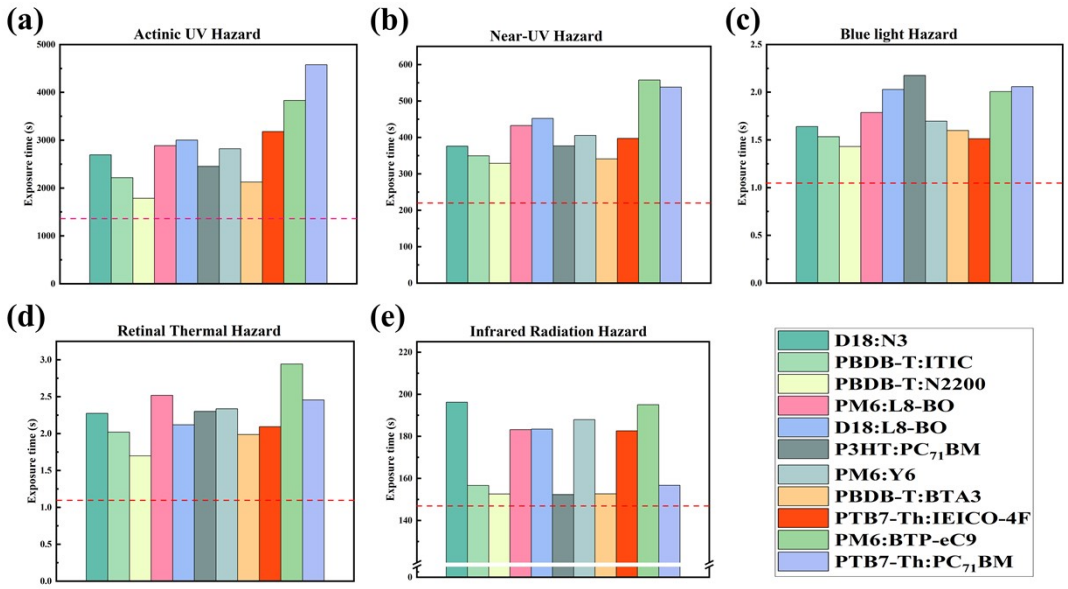

Figure S2. Exposure time of organic ST-PV active layers for (a) actinic UV hazard, (b) near-UV hazard, (c) blue light hazard, (d) infrared radiation hazard, and (e) retinal thermal hazard. The red dotted line corresponds to the sunlight exposure time.

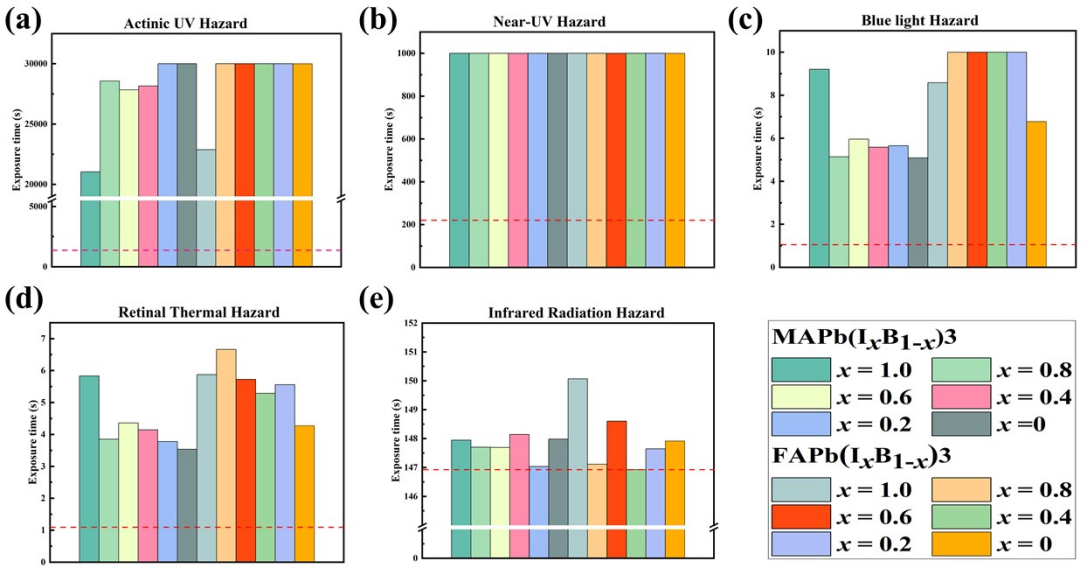

Figure S3. Exposure time of perovskite ST-PV active layers for (a) actinic UV hazard, (b) near-UV hazard, (c) blue light hazard, (d) infrared radiation

hazard, and (e) retinal thermal hazard. The red dotted line corresponds to the sunlight exposure time.

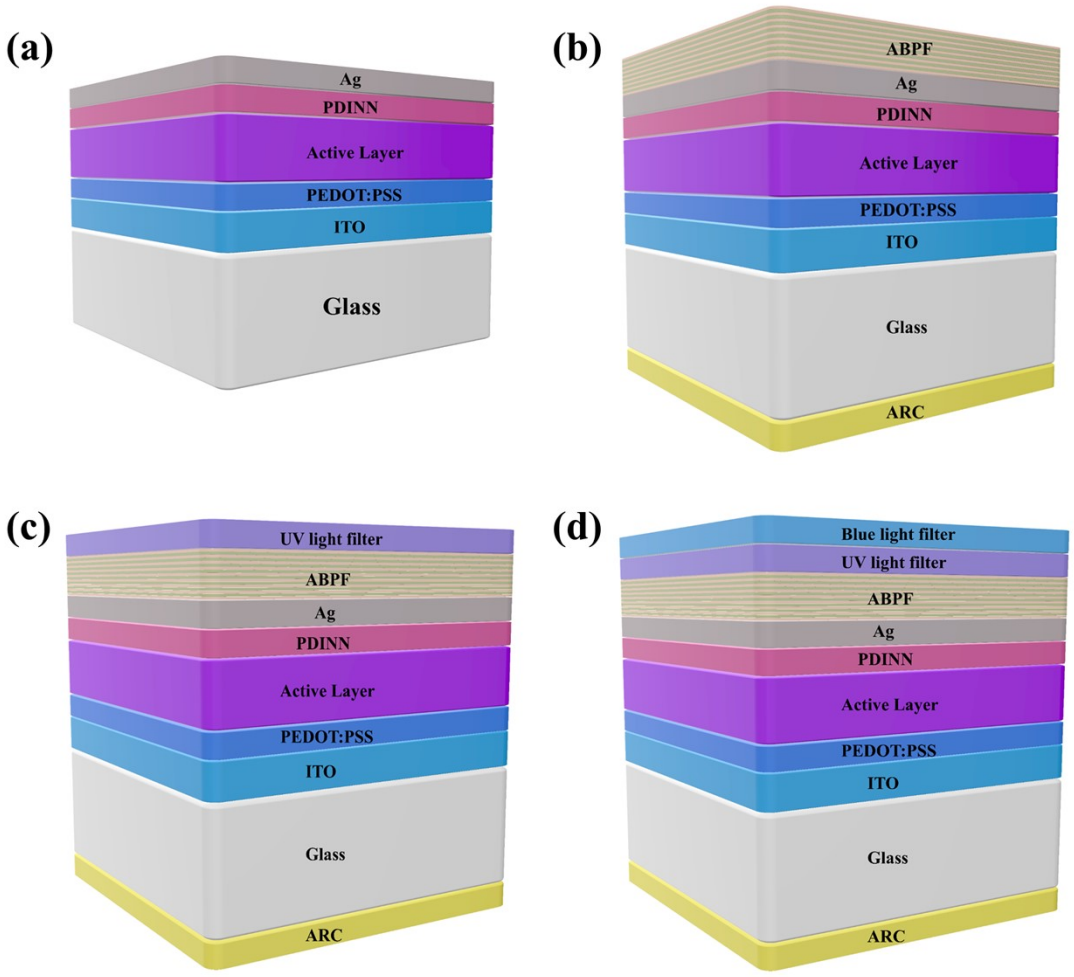

Figure S4. Schematic diagram of (a) standard ST-OPV devices, (b) ST-OPV devices with ARC/ABPF, (c) ST-OPV devices with ARC/ABPF/UV filter and (d) ST-OPV devices with ARC/ABPF/UV filter/blue light filter.

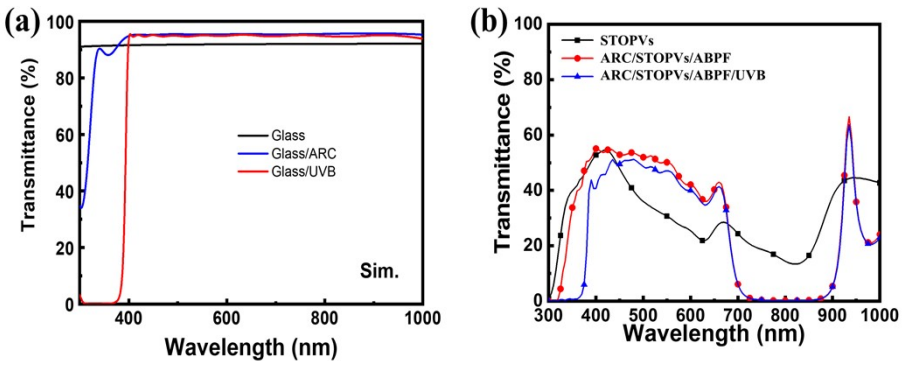

Figure S5. The transmittance spectra of (a) glass with and without different filters and (b) STOPV devices with and without different structures.

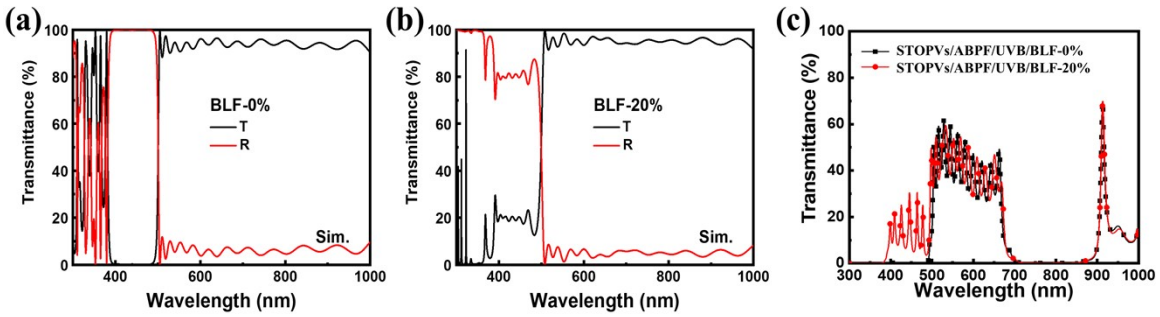

Figure S6. The simulated transmittance (T) and reflective (R) curves of (a) BLF-0% filter, (b) BLF-20% filter and (c) STOPV devices with these filters.

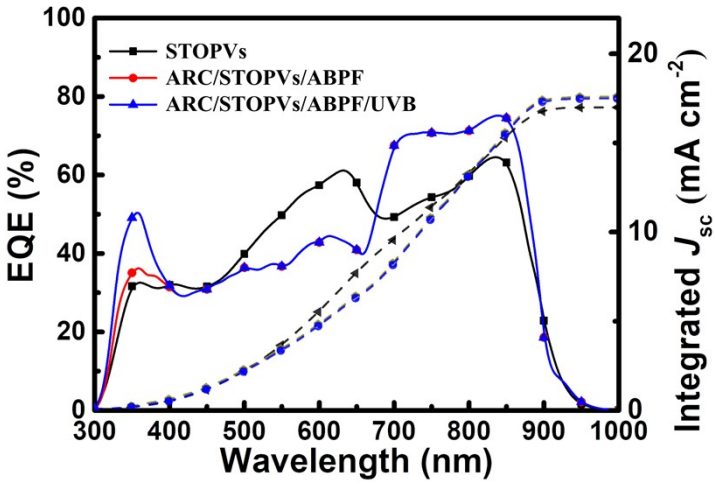

Figure S7. Summary plots of EQE and J_{sc} for STOPVs with different structures.

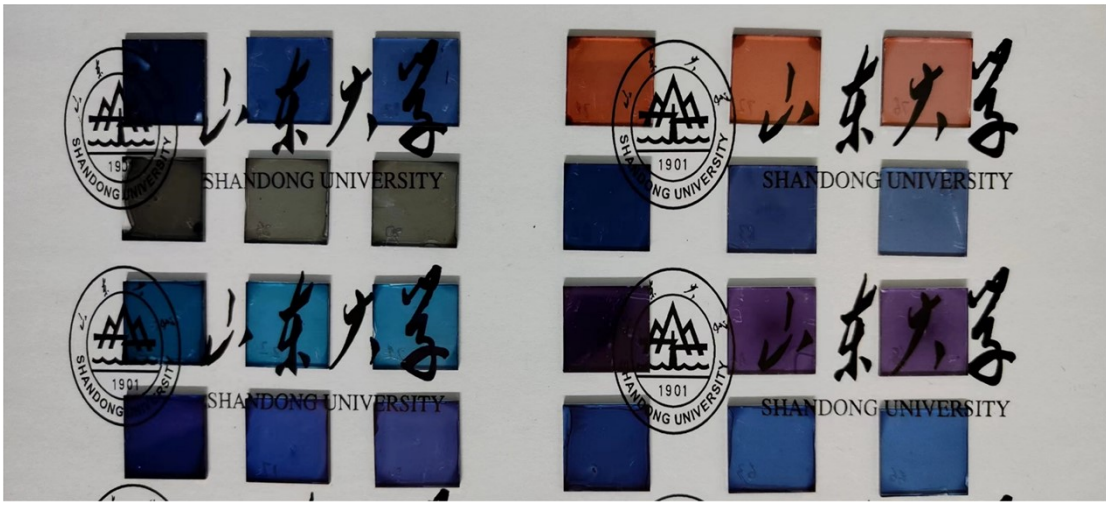

Figure S8. Digital photographs of some organic ST-PV films with different thickness.

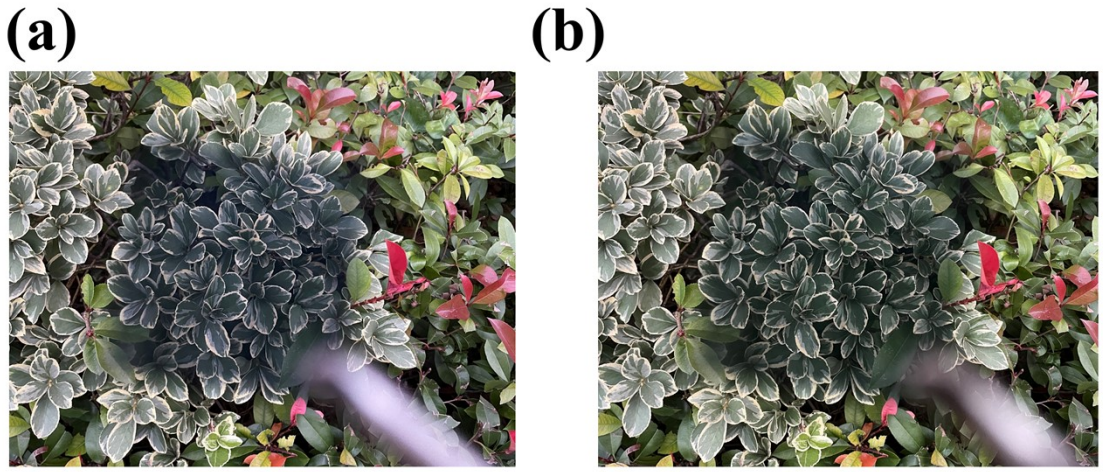

Figure S9. Digital photographs of (a) ARC/STOPVs/ABPF device and (b) ARC/STOPVs/ABPF/ UV filter / blue light filter device.

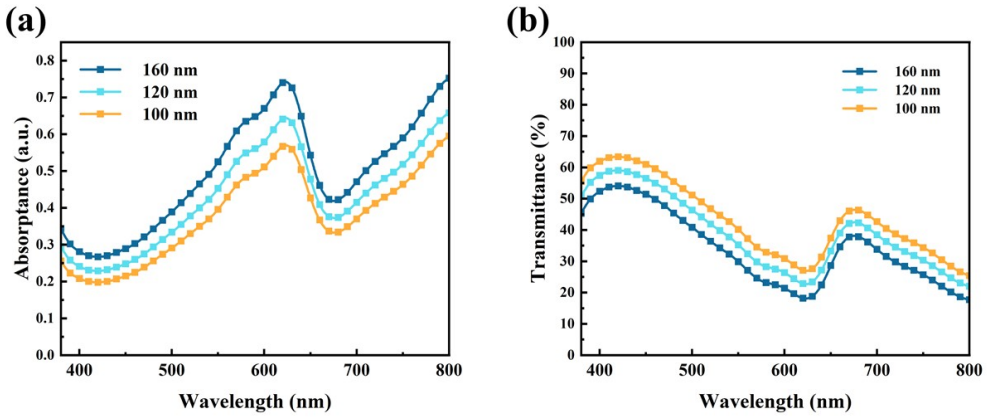

Figure S10. The absorption spectra and transmittance spectra of PM6:Y6.

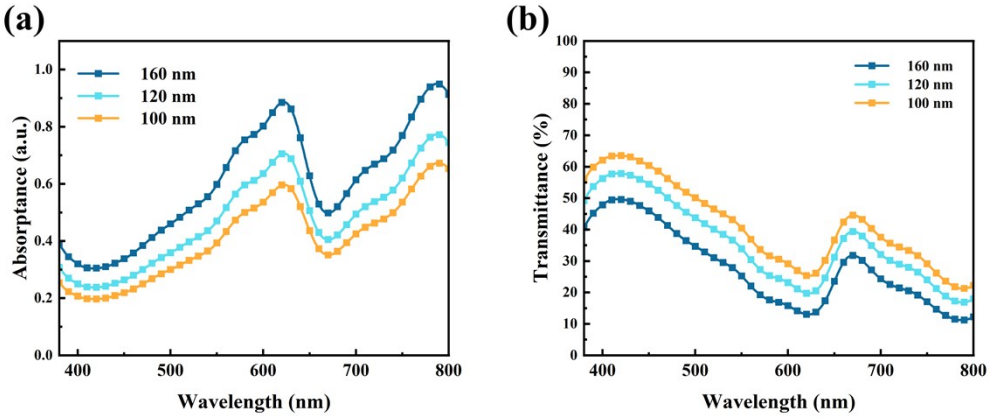

Figure S11. The absorption spectra and transmittance spectra of PM6:L8-BO.

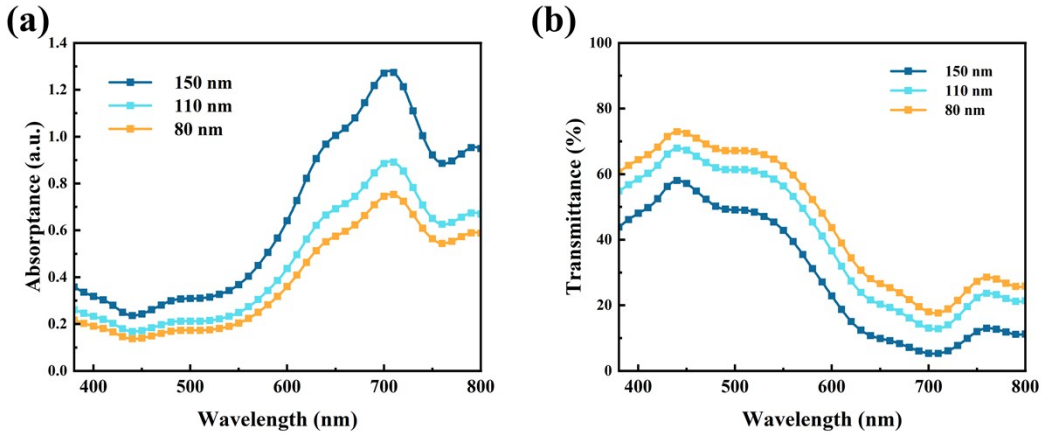

Figure S12. The absorption spectra and transmittance spectra of PBDB-T:IEICO-4F.

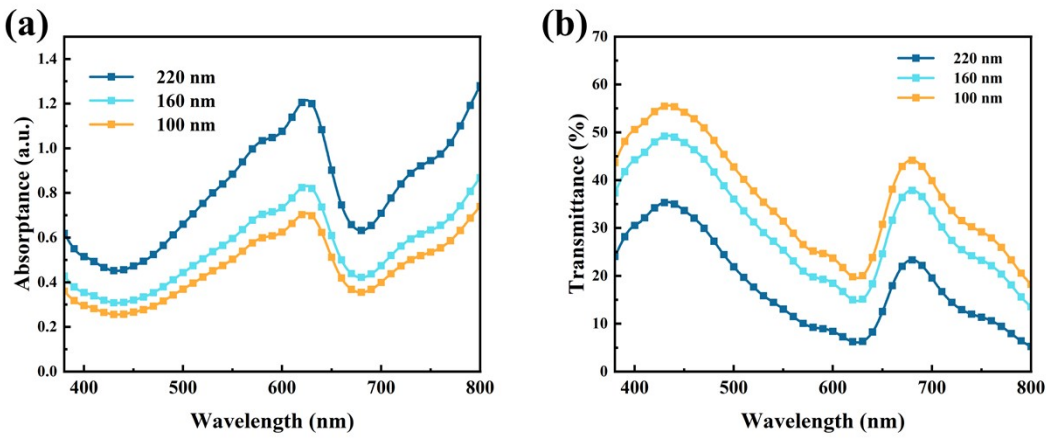

Figure S13. The absorption spectra and transmittance spectra of PM6:BTP-eC9.

Figure S14. The absorption spectra and transmittance spectra of D18:N3.

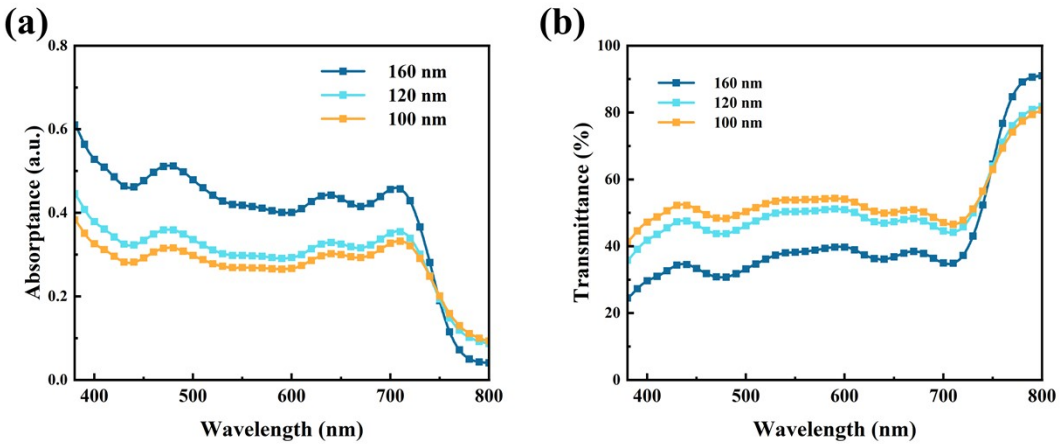

Figure S15. The absorption spectra and transmittance spectra of PTB7-Th:$PC_{71}BM$.

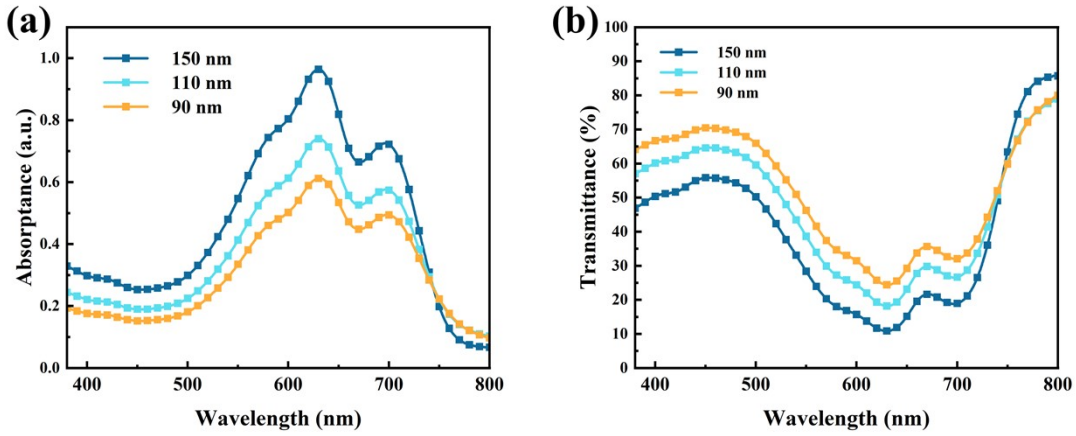

Figure S16. The absorption spectra and transmittance spectra of PBDB-T:ITIC.

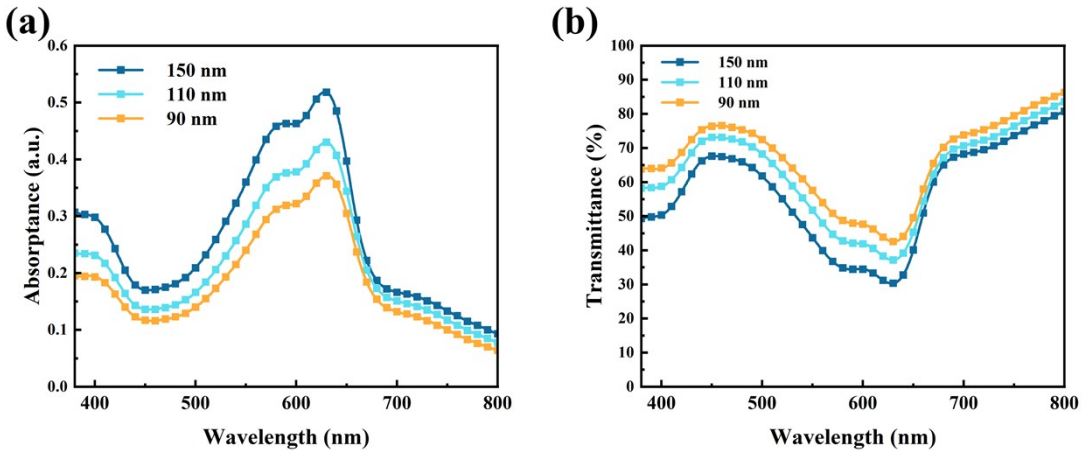

Figure S17. The absorption spectra and transmittance spectra of PBDB-T:N2200.

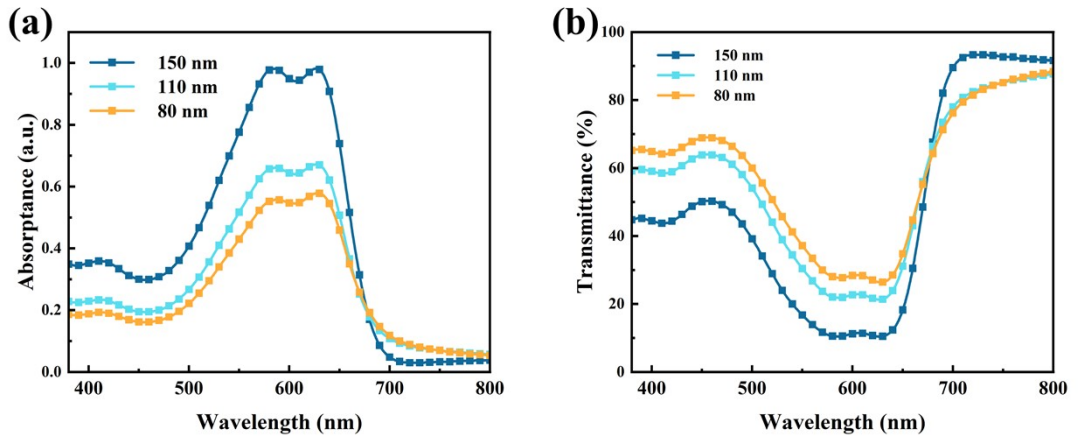

Figure S18. The absorption spectra and transmittance spectra of PBDB-T:BTA3.

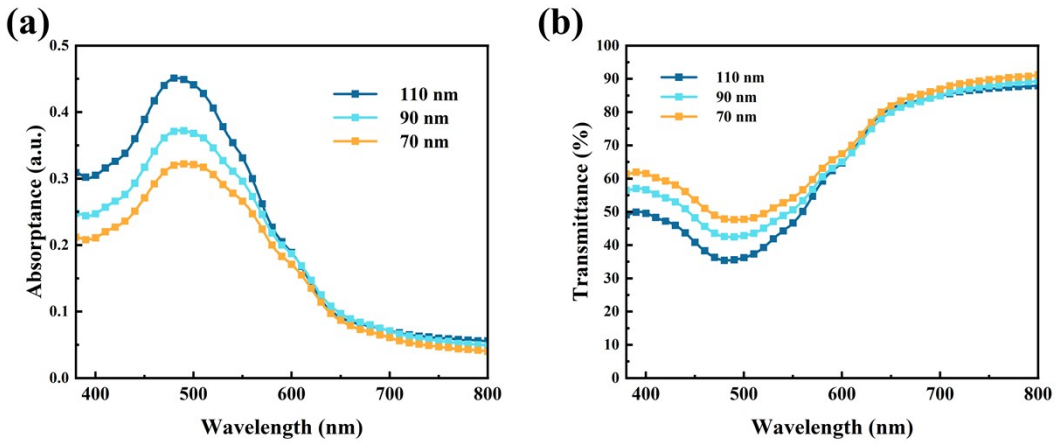

Figure S19. The absorption spectra and transmittance spectra of P3HT:$PC_{71}BM$.

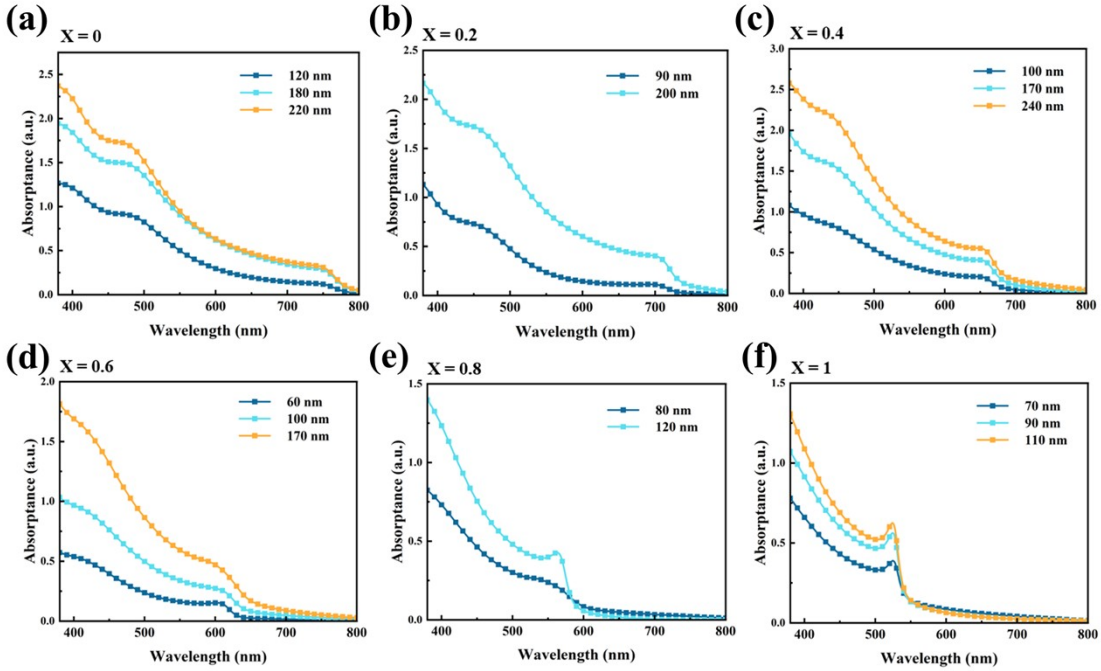

Figure S20. Absorption spectra of $MAPb(I_{1-x}Br_x)_3$ perovskite films where X is (a) 0, (b) 0.2, (c) 0.4, (d) 0.6, (e) 0.8 and (f) 1.

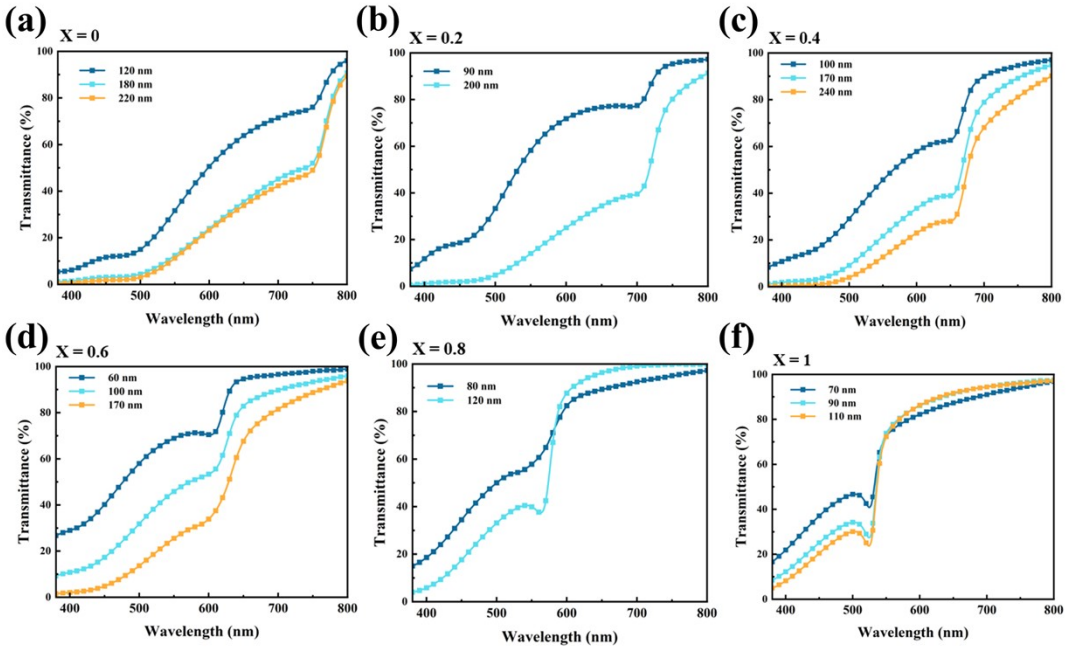

Figure S21. Transmittance spectra of $MAPb(I_{1-x}Br_x)_3$ perovskite films where X is (a) 0, (b) 0.2, (c) 0.4, (d) 0.6, (e) 0.8 and (f) 1.

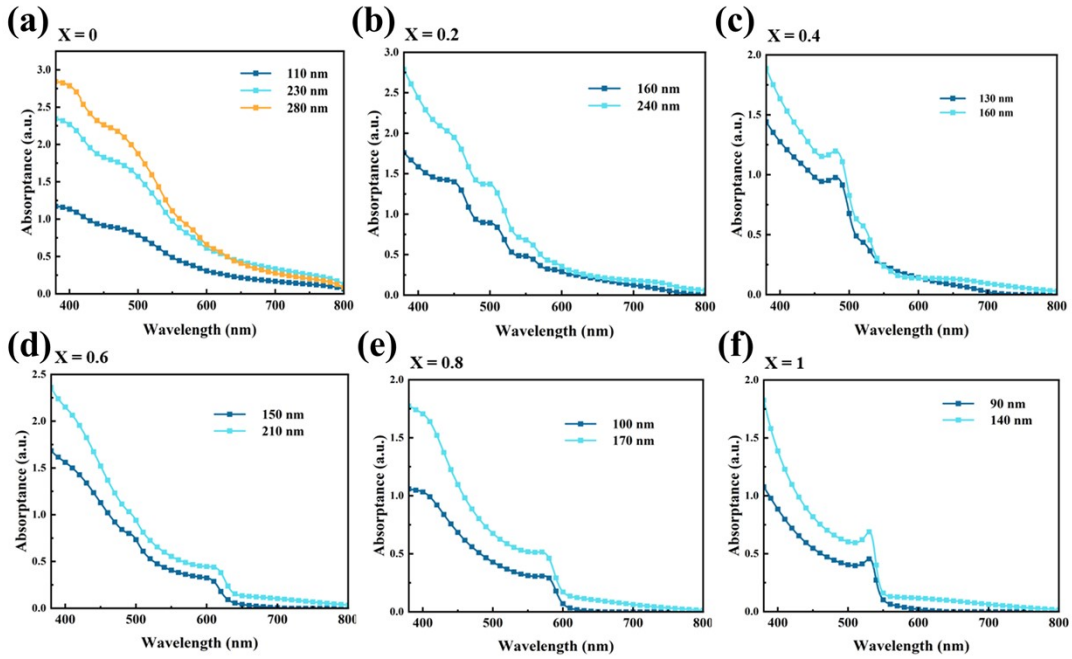

Figure S22. Absorption spectra of $FAPb(I_{1-x}Br_x)_3$ perovskite films where X is (a) 0, (b) 0.2, (c) 0.4, (d) 0.6, (e) 0.8 and (f) 1.

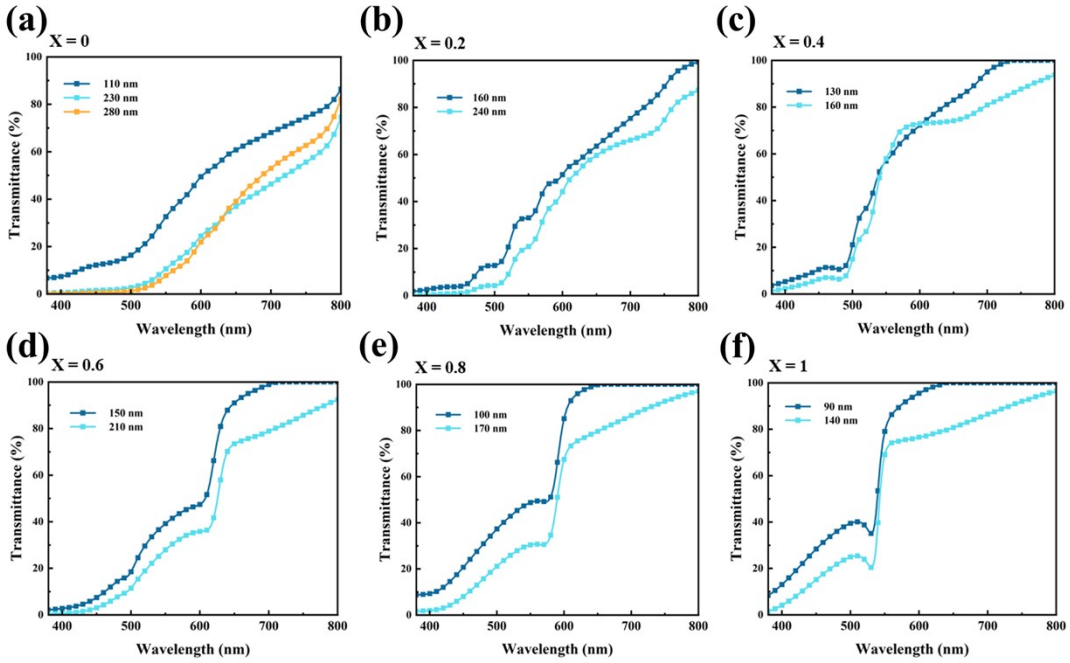

Figure S23. Transmittance spectra of $FAPb(I_{1-x}Br_x)_3$ perovskite films where X is (a) 0, (b) 0.2, (c) 0.4, (d) 0.6, (e) 0.8 and (f) 1.

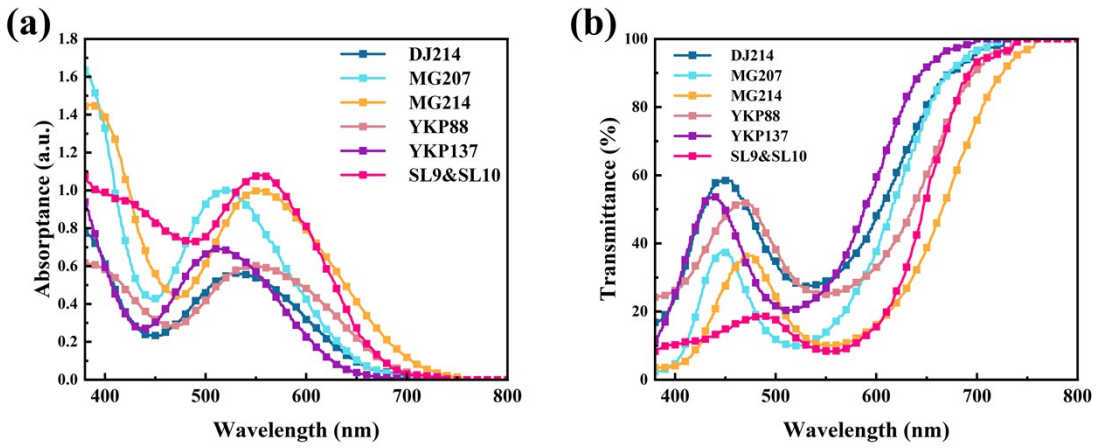

Figure S24. The absorption spectra and transmittance spectra of DSSC films.

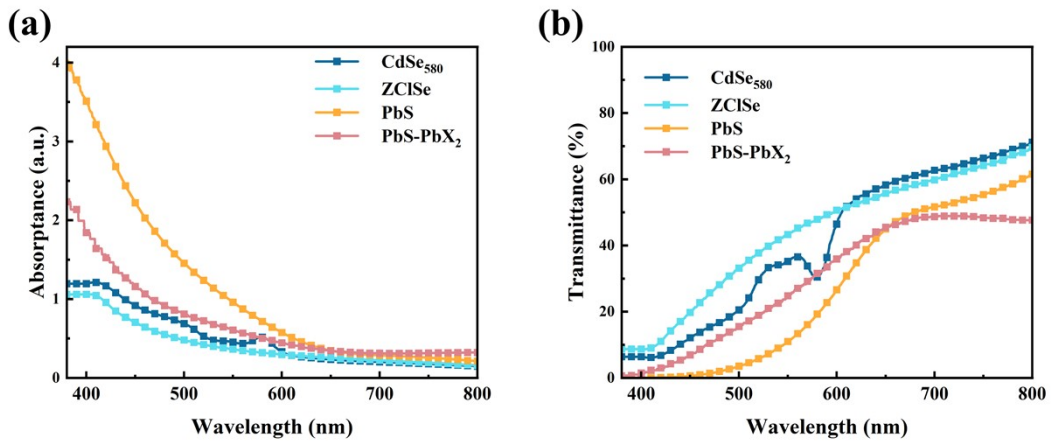

Figure S25. The absorption spectra and transmittance spectra of QSC films.

Reference

[1] W. Wang, W. Feng, J. Du, W. Xue, L. Zhang, L. Zhao, Y. Li, X. Zhong, Advanced Materials, 2018, 30, 1705746.

[2] M. Godfroy, J. Liotier, V. M. Mwalukuku, D. Joly, Q. Huaulme, L. Cabau, C. Aumaitre, Y. Kervella, S. Narbey, F. Oswald, E. Palomares, C. A. Gonzalez Flores, G. Oskam, R. Demadrille, Sustainable Energy & Fuels, 2021, 5, 144-153.

[3] Y. Ren, D. Zhang, J. Suo, Y. Cao, F. T. Eickemeyer, N. Vlachopoulos, S. M. Zakeeruddin, A. Hagfeldt, M. Graetzel, Nature, 2022, 613, 60-65.

[4] L. A. A. Pettersson, L. S. Roman, O. Inganäs, Journal of Applied Physics, 1999, 86, 487-496.

[5] K.-S. Chen, J.-F. Salinas, H.-L. Yip, L. Huo, J. Hou, A. K. Y. Jen, Energy & Environmental Science, 2012, 5, 9551-9557.

References in Figure 7

[1] M. Godfroy, J. Liotier, V. M. Mwalukuku, D. Joly, Q. Huaulme, L. Cabau, C. Aumaitre, Y. Kervella, S. Narbey, F. Oswald, E. Palomares, C. A. Gonzalez Flores, G. Oskam, R. Demadrille, Sustainable Energy & Fuels 2021, 5, 144.

[2] W. Chen, J. Zhang, G. Xu, R. Xue, Y. Li, Y. Zhou, J. Hou, Y. Li, Advanced Materials 2018, 30, 1800855.

[3] H. T. Dastjerdi, P. Qi, Z. Fan, M. M. Tavakoli, Acs Applied Materials & Interfaces 2020, 12, 818.

[4] Y. Chang, X. Zhu, L. Zhu, Y. Wang, C. Yang, X. Gu, Y. Zhang, J. Zhang, K. Lu, X. Sun, Z. Wei, Nano Energy 2021, 86, 106098.

[5] Y. Guo, K. Shoyama, W. Sato, E. Nakamura, Advanced Energy Materials 2016, 6, 1502317.

[6] M. T. Horantner, P. K. Nayak, S. Mukhopadhyay, K. Wojciechowski, C. Beck, D. McMeekin, B. Kamino, G. E. Eperon, H. J. Snaith, Advanced Materials Interfaces 2016, 3, 1500837.

[7] Z. Hu, J. Wang, X. Ma, J. Gao, C. Xu, X. Wang, X. Zhang, Z. Wang, F. Zhang, Journal of Materials Chemistry A 2021, 9, 6797.

[8] Z. Hu, J. Wang, Z. Wang, W. Gao, Q. An, M. Zhang, X. Ma, J. Wang, J. Miao, C. Yang, F. Zhang, Nano Energy 2019, 55, 424.

[9] Z. Hu, Z. Wang, F. Zhang, Journal of Materials Chemistry A 2019, 7, 7025.

[10] X. Huang, L. Zhang, Y. Cheng, J. Oh, C. Li, B. Huang, L. Zhao, J. Deng, Y. Zhang, Z. Liu, F. Wu, X. Hu, C. Yang, L. Chen, Y. Chen, Advanced Functional Materials 2022, 32, 2108634.

[11] H. I. Jeong, S. Biswas, S. C. Yoon, S.-J. Ko, H. Kim, H. Choi, Advanced Energy Materials 2021, 11, 2102397.

[12] B.-H. Jiang, H.-E. Lee, J.-H. Lu, T.-H. Tsai, T.-S. Shieh, R.-J. Jeng, C.-P. Chen, Acs Applied Materials & Interfaces 2020, 12, 39496.

[13] J. W. Jung, C.-C. Chueh, A. K. Y. Jen, Advanced Energy Materials 2015, 5, 1500486.

[14] H.-C. Kwon, A. Kim, H. Lee, D. Lee, S. Jeong, J. Moon, Advanced Energy Materials 2016, 6, 1601055.

[15] F. R. Li, Y. Xu, W. Chen, S. H. Xie, J. Y. Li, Journal of Materials Chemistry A 2017, 5, 10374.

[16] Y. Li, C. Ji, Y. Qu, X. Huang, S. Hou, C.-Z. Li, L.-S. Liao, L. J. Cuo, S. R. Forrest, Advanced Materials 2019, 31, 1903173.

[17] Y. Li, J.-D. Lin, X. Che, Y. Qu, F. Liu, L.-S. Liao, S. R. Forrest, Journal of the

American Chemical Society 2017, 139, 17114.

[18] Q. Liu, L. G. Gerling, F. Bernal-Texca, J. Toudert, T. Li, X. Zhan, J. Martorell, Advanced Energy Materials 2020, 10, 1904196.

[19] W. Liu, S. Sun, S. Xu, H. Zhang, Y. Zheng, Z. Wei, X. Zhu, Advanced Materials 2022, 34, 2200337.

[20] J.-H. Lu, Y.-L. Yu, S.-R. Chuang, C.-H. Yeh, C.-P. Chen, Journal of Physical Chemistry C 2016, 120, 4233.

[21] X. Ma, Z. Xiao, Q. An, M. Zhang, Z. Hu, J. Wang, L. Ding, F. Zhang, Journal of Materials Chemistry A 2018, 6, 21485.

[22] C. Roldan-Carmona, O. Malinkiewicz, R. Betancur, G. Longo, C. Momblona, F. Jaramillo, L. Camacho, H. J. Bolink, Energy & Environmental Science 2014, 7, 2968.

[23] Y. Xie, Y. Cai, L. Zhu, R. Xia, L. Ye, X. Feng, H.-L. Yip, F. Liu, G. Lu, S. Tan, Y. Sun, Advanced Functional Materials 2020, 30, 2002181.

[24] Y. Xie, L. Huo, B. Fan, H. Fu, Y. Cai, L. Zhang, Z. Li, Y. Wang, W. Ma, Y. Chen, Y. Sun, Advanced Functional Materials 2018, 28, 1800627.

[25] Y. Xie, R. Xia, T. Li, L. Ye, X. Zhan, H.-L. Yip, Y. Sun, Small Methods 2019, 3, 1900424.

[26] X. Zhang, D. Jia, C. Hagglund, V. A. Oberg, J. Du, J. Liu, E. M. J. Johansson, Nano Energy 2018, 53, 373.

[27] J. Zhao, K. O. Brinkmann, T. Hu, N. Pourdavoud, T. Becker, T. Gahlmann, R. Heiderhoff, A. Polywka, P. Goerrn, Y. Chen, B. Cheng, T. Riedl, Advanced Energy Materials 2017, 7, 1602599.

[28] S. Guan, Y. Li, K. Yan, W. Fu, L. Zuo, H. Chen, Advanced Materials 2022, 34, 2205844.